RAPID COMMUNICATIONS

PHYSICAL REVIEW E VOLUME 52, NUMBER 6 DECEMBER 1995

Secondary instability in surface-tension-driven Bénard convection

K. Nitschke* and A. Thess*
Forschungszentrum Rossendorf, P.O. Box 510 119, 01314 Dresden, Germany
(Received 16 January 1995)

We report accurate experimental investigations of surface-tension-driven Bénard convection extending up to $\varepsilon=(\Delta T-\Delta T_c)/\Delta T_c=4.5$ into the supercritical range. The measurements are performed in a circular box with an aspect ratio of 23. At $\varepsilon_S=2.35\pm0.40$ hexagonal cells, perfectly organized at the onset of the primary instability, lose stability and are gradually replaced by square cells. The transition process is mediated by pentagons.

PACS number(s): 47.20.Dr, 47.54.+r

Studies on pattern formation and turbulence in nonisothermal fluids are mainly focused on the buoyancy driven Rayleigh-Bénard convection (RBC), although the classical experiments of Bénard [1] were predominantly driven by surface tension [2,3]. While experimental investigations of RBC have been performed up to $\varepsilon=(\Delta T-\Delta T_c)/\Delta T_c=10^{13}$ by Libchaber *et al.* (see [4] for a review; ΔT_c is the critical temperature difference), experiments in surface-tension-driven Bénard convection (BC) have been restricted to the weakly supercritical regime. This is due to the fact that the requirement of a small layer depth, necessary for the dominance of surface tension over buoyancy, imposes severe constraints on the maximum of ε. We have extended the accurate measurements of Koschmieder *et al.* [5] up to $\varepsilon=4.5$ into the nonlinear regime, which permitted us to study the nonlinear evolution of the hexagonal planform in BC at larger distances from the instability threshold. The goal of the present paper is to report an experimental identification of a secondary instability, at which a pattern of hexagonal cells loses its stability against square convection cells.

On the theoretical side, the absence of reflection symmetry and the location of the driving force at the free surface are sources for an increased complexity of BC in comparison to RBC. Although considerable effort toward the understanding of BC has been undertaken in the past [5–10], our knowledge about the nonlinear evolution of hexagonal Bénard cells and their secondary instabilities is far from complete. A systematic theoretical investigation of the secondary instabilities of hexagonal cells in BC is still lacking, in contrast to RBC where Busse's [11] comprehensive theory provides a rather complete insight into the secondary instabilities of rolls. Recent theoretical works on amplitude instabilities [9,12] and phase instabilities [9] of hexagons in BC predict a successive replacement of hexagons by rolls for $\varepsilon=O(1)$. However, these predictions should be considered with caution due to the limited validity of amplitude equation models in this range.

Our experiments are performed with a 10 cS (centistoke) silicone oil (NM 10, Hüls AG) whose Prandtl number Pr $=100$ at $T=25$ °C. We use a cylindrical cell (radius $r=35.0$ mm) with walls made of Plexiglas. The fluid height is $d=1.55\pm0.02$ mm, leading to an aspect ratio $\Gamma=r/d=23$. The bottom of the chamber consists of a polished silicon crystal on a 5 cm thick copper block. As upper plate of the chamber, we use a sapphire window. The air gap between fluid and sapphire is 0.40 mm. Care is taken in minimizing lateral temperature gradients by placing the copper block in a prevacuum. The sapphire window is cooled by an axisymmetric water flow (temperature stability ±0.01 K). In order to visualize the convection pattern we use a shadowgraph technique coupled to a digital image processing system with a resolution of $768\times512\times8$ bit.

The determination of the temperature difference ΔT across the fluid layer is more difficult than in RBC due to the presence of the thin air layer, whose convective state is not amenable to direct measurement. We determine ΔT by measuring the temperature of the fluid bottom and of the cooling water both before and after circulating over the sapphire window [13]. From the latter two quantities we calculate the heat flux. Taking into account the known heat conductivities and thickness of sapphire and oil layer, together with the thickness and a hypothetic conductivity of the air layer, we evaluate ΔT. All temperature measurements are performed with quartz crystals. This method yields a precision of 12% in the determination of ΔT.

For the heating of the fluid bottom we use an electrical resistor whose power supply is regulated by means of a PC interface. In order to ensure a quasistatic regime, the rise of the bottom temperature is limited to 0.07 K per hour. Moreover, the temperature is kept constant for one horizontal relaxation time $\tau_h=r^2/\kappa$ (approximately 3.4 hours) before taking a shadowgraph image. Thus, the typical time span for one experiment is nearly $100\tau_h$.

Linear stability theory [3], applied to the conditions of our system, predicts instability if $\Delta T>0.89$ K, which corresponds to a Marangoni number $\mathrm{Ma}_c=(d\sigma/dT)\Delta T_c d/\rho\nu\kappa=76.4$ and to a Rayleigh number of $\mathrm{Ra}_c=(d\rho/dT)g\Delta T_c d^3/\rho\nu\kappa=30.6$ for a fluid with a perfectly insulating surface. σ,ρ,ν,κ,g denote surface tension, density, kinematic viscosity, thermal diffusivity, and gravitational acceleration, respectively. Note that Ma is by a temperature-independent factor 2.5 larger than Ra, expressing the dominance of surface tension over buoyancy. Several checks were made in order to test the quality of the experimental facility. The critical Marangoni number was reproduced within the precision of the aforementioned method for deter-

*Present address: Institute for Fluid Mechanics, Dresden University of Technology, 01062 Dresden, Germany.

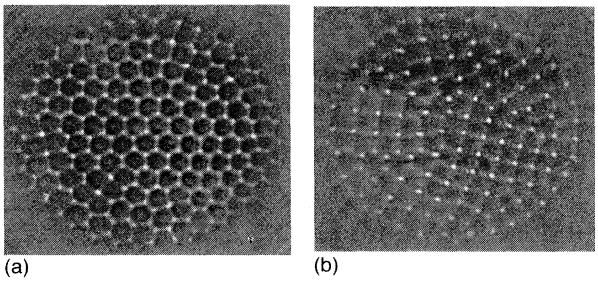

FIG. 1. Planform transition in surface-tension-driven Bénard convection: intensity corrected shadowgraph images of the hexagonal pattern for $\varepsilon = 2.4$ (a) and of the square pattern for $\varepsilon = 3.8$ after evolution according to the first transition route (b).

mining ΔT. The critical wave number was 6% higher than the critical one due to the finite Γ in agreement with [14].

Figures 1(a) and 1(b) provide a first glimpse of the transition from hexagonal to square planform in BC, which constitutes the main result of our work. The experiments start with a hexagonal pattern, which is well ordered at the onset of the primary instability and can be kept stable up to approximately $\varepsilon \sim 2.4$ [Fig. 1(a)]. The shadowgraph intensity at the cell boundaries increases monotonically with ε and, above $\varepsilon \sim 2.5$, is accompanied by an even stronger growth of the intensity at the cell knots as highlighted in Fig. 2. Beyond $\varepsilon \sim 3.4$, the convective cells appear as an arrangement of bright spots, corresponding to the cell knots, in the shadowgraph image [Fig. 1(b)]. Qualitatively similar phenomena have been observed in the direct numerical simulation of Ref. [10] for BC. Above $\varepsilon = 2.35 \pm 0.40$ (see below) we observe a smooth transition from hexagonal convection cells to square cells. Figure 1(b) shows a state consisting of two domains with square cells. In order to quantitatively characterize the transition process we consider the power spectral density $P(k,\varphi)$, belonging to the shadowgraph intensity fields in Fig. 1, where k and φ denote the polar coordinates in the two-dimensional wave number space. Following Ref. [15] we evaluate the azimuthal distribution $Q(\varphi)$ of the power spectral density P,

$$Q(\varphi) = \frac{1}{W} \int_{k_1}^{k_2} dk\ kP(k,\varphi), \tag{1}$$

where W is a normalization factor. The domain of radial integration is restricted to the immediate vicinity of the main

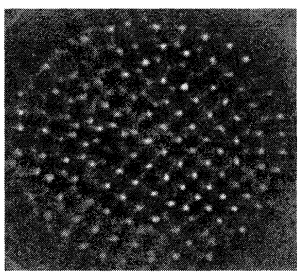

FIG. 2. Shadowgraph image for $\varepsilon = 2.8$ showing the coexistence of hexagons and squares during the evolution according to the second transition route.

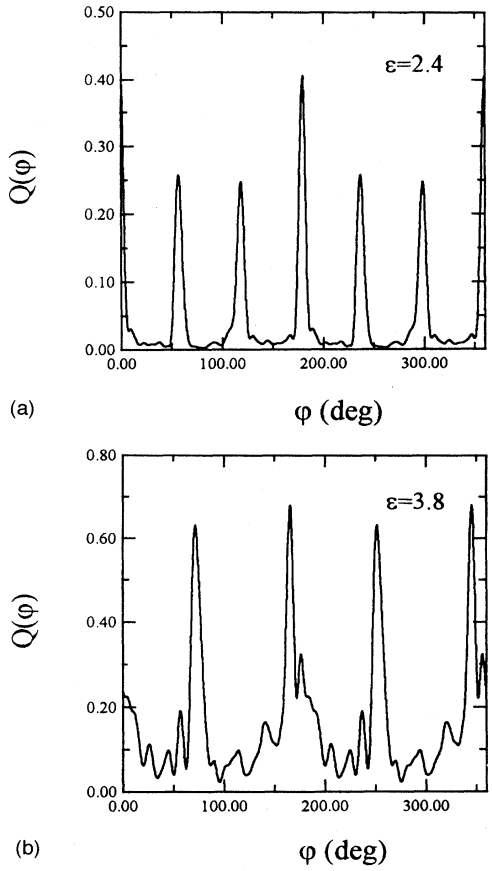

FIG. 3. The symmetry changes during the hexagon-square transition: azimuthal distribution of the power spectral density for $\varepsilon = 2.4$ (a) and $\varepsilon = 3.8$ (b).

peaks. Higher harmonics are filtered out using a binomial filter. Figure 3 quantitatively affirms the visually observed transition from the sixfold symmetry, in which the wave vectors of the main peaks are separated by an angle of 60°, to the fourfold symmetry with an angle of 90° between the main peaks. Although the pattern of Fig. 1(b) underlying Fig. 3(b) consists of two differently oriented domains of square cells, the fourfold symmetry is well reflected by $Q(\varphi)$. The reason for the nonequipartition of the shadowgraph intensity among the peaks in Fig. 3(a) is not entirely obvious. However, we did not find any systematic preference for particular peaks in different experimental runs.

After having characterized its integral properties, let us consider the transition from a local point of view. We found the elementary process to occur via gradual merging of cell knots as sketched in Fig. 4, which was generated from two digitized shadowgraph images. Adjoining cell knots, two pairs of which are highlighted by arrows, of a hexagonal cell move towards each other [Fig. 4(a)]. The approach of the knots proceeds with different speed in the particular pairs. Consequently, a pentagon is formed in an intermediate step before a square cell [Fig. 4(b)] is attained.

We have identified two routes by which the square cells invade the initially hexagonal convective pattern. In the first one, which is observed in 8 of 10 experiments, the transformation of hexagons into pentagons starts at five points lo-

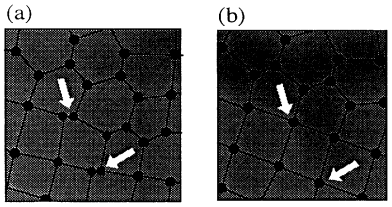

FIG. 4. Merging of cell knots during the hexagon-square-transition for $\varepsilon=3.4$ (a) and $\varepsilon=3.5$ (b).

cated along the circumference of the fluid. The pentagons spread into the still hexagonal domain, leaving squares behind. Figure 1(b) shows the final result of this route. In the second route the transformation of hexagons into pentagons starts at only one location in the vicinity of the wall. A straight front of pentagons moves through the container, converting hexagons into pentagons. The coexistence of hexagons and squares in this regime can be seen in Fig. 2. The cause for the appearance of the two distinct scenarios is not entirely obvious. It can be speculated that the second route is triggered by a small angle between the sapphire plate and the fluid surface, slightly increasing locally the temperature difference across the layer.

Next we turn to the characterization of the composition of the pattern, comprising different amounts of hexagons, pentagons, and squares, during the hexagon-square transition. To this end we introduce the quantities $p_i=N_i/N$ $(i=4,5,6)$ where the N_i represent the number of squares $(i=4)$, pentagons $(i=5)$, and hexagons $(i=6)$, respectively. N stands for the total number of cells in the container, excluding the "incomplete" cells along the rim. Although care was taken in ensuring thermal equilibration we have to note a considerable scatter between the p_i of different experimental runs. This is likely to be an intrinsic feature of the system rather than a deficiency of the experimental apparatus, indicating the existence of a multitude of quasiequilibria. As a result of the defect dynamics taking place in the evolving convective structure, we observe, above $\varepsilon\sim1$, a decrease of the hexagon number [Fig. 5(a)]. As evident from Fig. 5(b) the overall loss of hexagons is approximately equal to the gain of pentagons. Above $\varepsilon\sim2.3$ this transformation is accompanied by the transformation of pentagons into squares, the amount of which starts to grow [Fig. 5(c)]. We wish to remark that a small percentage of cells, especially those connecting domains of square cells with different orientation, has a tetragonal rather than a square planform. The special role of the pentagons as the catalyzing elements of the transition is displayed in Fig. 5(b). The number of pentagons reaches a maximum at $\varepsilon=3.4\pm0.6$ which coincides approximately with the maximum slope of the square and hexagon numbers. An unambiguous determination of the number of edges is in some cases not possible due to a very small distance between two adjoining cell knots. This is the cause for a small deviation of the measured quantities from the normalization condition $p_4+p_5+p_6=1$. An exact determination of the critical value for the onset of the hexagon-square transition is difficult. Due to the continuous character of the transition, the change in the heat transport connected with the appearance of square cells is so small in the early stages that it cannot be reliably detected in our Nusselt number

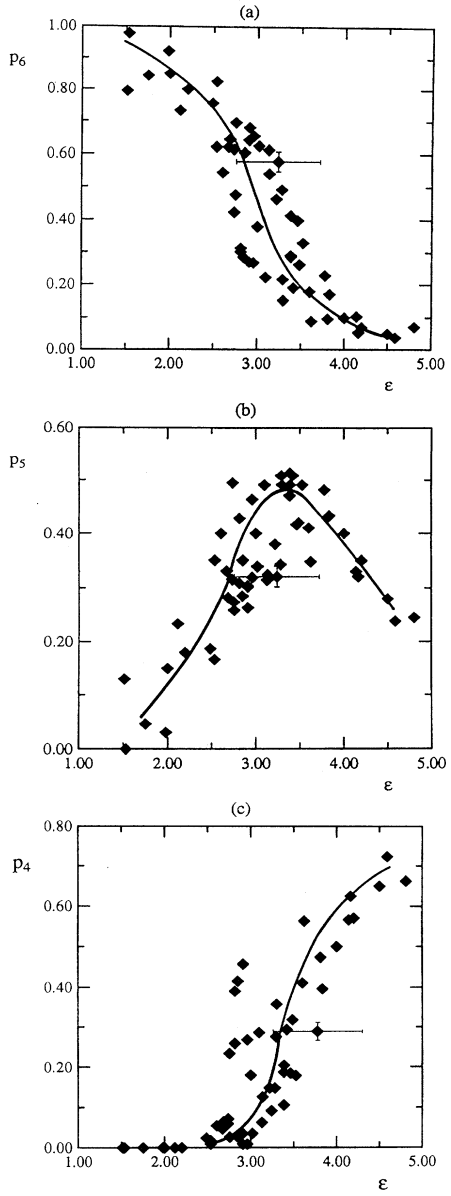

FIG. 5. Dependence of the number of hexagons p_6 (a), pentagons p_5 (b), and squares p_4 (c), on ε. The diagrams contain the results of seven different independent experimental runs. The lines are drawn to guide the eye.

measurements. In order to give a quantitative measure for the onset of the secondary instability we apply a linear least-square fit to the number of square cells as a function of ε in the interval $2.0<\varepsilon<4.0$ [cf. Fig. 5(c)]. This gives $p_4=0.29\varepsilon-0.68$ which provides the threshold $\varepsilon_s=2.35\pm0.40$ for the hexagon-square transition. The uncertainty of 17% in the determination of ε is caused both by the error in the determination of ΔT and by the nonuniqueness of the fit. Note that p_4 cannot serve as an order parameter with the hypothetic square root behavior, because the ideal transition would proceed directly from hexagons to squares, i.e., $p_4=0$ for $\varepsilon<\varepsilon_S$ and $p_4=1$ for $\varepsilon>\varepsilon_S$, as shall be discussed at the end of this paper.

In order to check the robustness of the observed phenomena, several other silicone oils have been tested. Experiments with an oil of a different manufacturer (Wacker Chemie AG), having the same Pr, brought only shifts within the error of the previous measurements. In order to exclude transient effects we performed an experiment in which $\varepsilon=3.5$ was held constant over a time span of $40\tau_h$, much larger than the thermal equilibration time ($1\tau_h$) of the previous experiments. The values of the p_i remained stable up to a scatter of $\pm 15\%$ with no tendency of p_5 to relax to smaller values. Using an oil with Pr=200, we observed the hexagon-square transition to be shifted to a higher ε, indicating the significance of the viscous properties of the fluid. A systematic investigation in fluids with Pr>200 is technically more difficult and constitutes the subject of ongoing investigations.

A specific difficulty of BC is the possibility of uncontrolled heat transfer enhancement due to convection in the air layer as well as increased evaporation of the oil due to a small but nonzero volatility. Our estimates, based on the numerical results of Ref. [10], show that the first effect is weak if the Péclet number in the air $\mathrm{Pe}_{\mathrm{air}}=c\varepsilon(\kappa\delta/\kappa_{\mathrm{air}}d)$ is small. Here c is a numerical factor of the order $c\sim 30-50$, κ_{air} is the heat diffusivity of the air, and δ the thickness of the air layer. Notice that even with the most pessimistic estimate $c=50$ we get, at our highest supercritical value $\varepsilon=4.5$, a value of $\mathrm{Pe}_{\mathrm{air}}\sim 0.3$, which is well below unity and which is comparable in magnitude to the experimental uncertainty of our temperature measurements.

The secondary instability observed in the present work differs markedly from other transitions which have been studied so far. None of the documented square patterns [16,17] evolves from a hexagonal planform, as in our case. In contrast to hexagon-roll competition in RBC with non-Boussinesq fluids [18], three planforms are involved in our transition.

A final comment is necessary on the possibility of a theoretical explanation of the hexagon-square transition. After we had finished this work, direct numerical simulations (DNS's) of BC [19] have confirmed the existence and robustness of the hexagon-square transition. Furthermore, very recent investigations of BC with amplitude equations [20] reflect this transition too and show the coexistence of hexagons and squares. Apart from DNS and amplitude equations, another obvious approach consists in the investigation of the secondary instabilities of hexagons following the method employed by Busse for the investigation of rolls in RBC [11]. It is likely that the most unstable mode responsible for the displacement of knots (cf. Fig. 4), and therefore for the transition from hexagons to squares, must be sought among the class of perturbations directed along one of the symmetry lines of the hexagonal lattice. Note that this ideal bifurcation, compatible with our observations from Fig. 4, proceeds directly from deformed hexagons (i.e., $p_6=1$, $p_4=0$) to tetragons (i.e., $p_6=0$, $p_4=1$). In a finite domain, only an imperfect bifurcation can occur which goes over the intermediate stage of a third planform.

The authors thank E. L. Koschmieder for his helpful comments in the early stage of the experiments, M. Bestehorn for stimulating discussions, and C. Perez-García and A. Golovin for communicating their results prior to publication. Financial support from the Sächsisches Staatsministerium für Wissenschaft und Kunst and from the Deutsche Forschungsgemeinschaft (Grant No. Th497/8-1) is gratefully acknowledged.

[1] H. Bénard J. Phys. (Paris) **9**, 513 (1900).
[2] M. J. Block, Nature (London) **178**, 650 (1956).
[3] J. R. Pearson, J. Fluid Mech. **4**, 489 (1958); D. A. Nield, *ibid.* **19**, 341 (1964).
[4] E. D. Siggia, Annu. Rev. Fluid Mech. **26**, 137 (1994).
[5] E. L. Koschmieder and D. W. Switzer, J. Fluid Mech. **240**, 533 (1992), and references therein.
[6] J. W. Scanlon and L. A. Segel, J. Fluid Mech. **30**, 149 (1969).
[7] P. Cerisier, C. Perez-Garcia, and R. Ocelli, Phys. Rev. A **47**, 3316 (1993), and references therein.
[8] A. Cloot and G. Lebon, J. Fluid Mech. **145**, 447 (1984).
[9] M. Bestehorn, Phys. Rev. E **48**, 3622 (1993).
[10] A. Thess and S. A. Orszag, J. Fluid Mech. **283**, 201 (1995).
[11] F. H. Busse, in *Hydrodynamic Instabilities and the Transition to Turbulence*, edited by H. L. Swinney and J. P. Gollub (Springer, Berlin, 1981), and references therein.
[12] J. Bragard and G. Lebon, Europhys. Lett. **21**, 831 (1993).
[13] E. L. Koschmieder, Rev. Sci. Instrum. **45**, 1164 (1974).
[14] P. Cerisier, C. Pérez-García, and J. Pantaloni, Phys. Rev. A **35**, 1949 (1987).
[15] J. P. Gollub and A. R. McCarriar, Phys. Rev. A **26**, 3470 (1982).
[16] P. Le Gal, A. Pocheau, and V. Croquette, Phys. Rev. Lett. **54**, 2501 (1985); E. Moses and V. Steinberg, *ibid.* **57**, 2018 (1986).
[17] E. L. Koschmieder, Beitr. Phys. Atmos. **39**, 1 (1966).
[18] S. Ciliberto, E. Pampaloni, and C. Pérez-García, Phys. Rev. Lett. **61**, 1198, (1988); E. Pampaloni, C. Pérez-Garcia, L. Albavetti, and S. Ciliberto, J. Fluid Mech. **234**, 393 (1992).
[19] M. Bestehorn, Phys. Rev. Lett. (to be published).
[20] C. Kubstrup, H. Herrero and C. Perez-García (unpublished); A. Golovin (private communication).

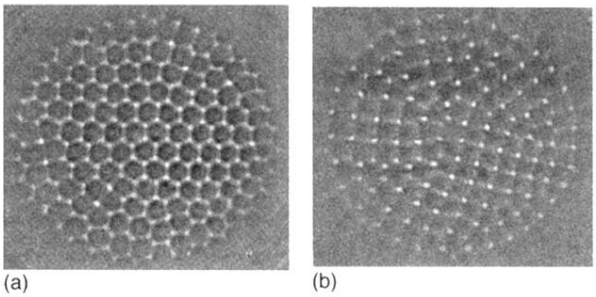

(a) (b)

FIG. 1. Planform transition in surface-tension-driven Bénard convection: intensity corrected shadowgraph images of the hexagonal pattern for $\varepsilon = 2.4$ (a) and of the square pattern for $\varepsilon = 3.8$ after evolution according to the first transition route (b).

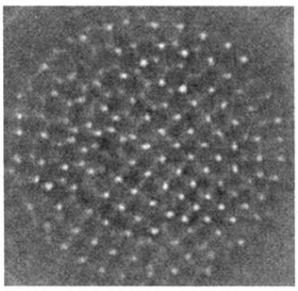

FIG. 2. Shadowgraph image for $\varepsilon = 2.8$ showing the coexistence of hexagons and squares during the evolution according to the second transition route.

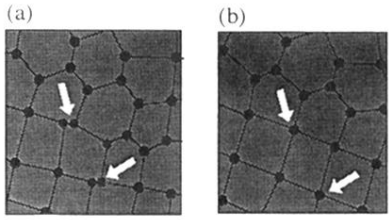

FIG. 4. Merging of cell knots during the hexagon-square-transition for $\varepsilon=3.4$ (a) and $\varepsilon=3.5$ (b).